Reducing Beam-Related Background on Forward Physics Detectors Using Crystal Collimation at the Large Hadron Collider[*]

D. Mirarchi[1,2,†] V. Avati,[3,2] R. Bruce,[2] M. Butcher,[2] M. D'Andrea[2,4] M. Di Castro,[2] M. Deile[2]
B. Dziedzic[5] K. Hiller,[6] S. Jakobsen[2] J. Kašpar,[7,2] K. Korcyl[5] I. Lamas[2] A. Masi,[2]
A. Mereghetti,[2] H. Garcia Morales[8,2,‡] Y. Gavrikov,[9,2] S. Redaelli,[2] B. Salvachua Ferrando,[2]
P. Serrano,[2] M. Solfaroli Camillocci,[2] and N. Turini[10]

[1]*The University of Manchester, Manchester M13 9PL, United Kingdom*
[2]*CERN, European Organization for Nuclear Research, Geneva 23 CH-1211, Switzerland*
[3]*AGH University of Science and Technology, Kraków, Poland*
[4]*Università degli Studi di Padova, Padova, Italy*
[5]*Institute of Nuclear Physics Polish Academy of Sciences, Krakow PL-31342, Poland*
[6]*Deutsches Elektronen-Synchrotron, Hamburg 22607, Germany*
[7]*Institute of Physics of the Academy of Sciences of the Czech Republic, Prague, Czech Republic*
[8]*Royal Holloway University of London, Egham Hill, Egham TW20 0EX, United Kingdom*
[9]*Petersburg Nuclear Physics Institute in National Research Centre "Kurchatov Institute" (PNPI), Gatchina, Russia*
[10]*Università degli Studi di Siena and Gruppo Collegato INFN di Siena, Siena, Italy*

Beam collimation in high-energy colliders is customarily carried out by means of massive amorphous absorbers surrounding the circulating beam. Several studies were performed in the last decades to establish an innovative collimation technique that relies on particle deflection by means of channeling between crystalline planes of a bent crystal. We report the operational use of crystal collimation in the Large Hadron Collider that was achieved during a special high-β^* physics run with low-intensity beams, representing a milestone for both accelerator and high-energy physics that could pave the way for new synergies in the near future. The deployment of this scheme was steered and motivated by machine-simulation studies, which were then confirmed experimentally using data provided by the experiments thanks to a sensitivity not accessible with the ring instrumentation. The evidence of beam-related experimental background reduction, improved data quality, and faster halo removal with respect to amorphous collimators is obtained using bent crystals as the primary collimation stage. A detailed description of preparatory studies and operational performance is reported, together with a comparison between experimental results and theoretical expectations.

I. INTRODUCTION

The CERN Large Hadron Collider (LHC) routinely stores and collides high-intensity proton beams [1]. Throughout run 2 (2015–2018), it was operated at a top

energy of 6.5 TeV. Apart from this standard operation, typically using beam intensities of a few 10^{14} protons, special runs are sometimes carried out. For example, the forward physics community required collisions at low energy. In October 2018 such a run was carried out at 450 GeV injection energy, using low-intensity beams (up to about 6×10^{11} protons per beam) and a special optics with a high β^* (the optical function at the interaction point) that was much larger than in standard operations. In particular, a β^* down to 25 cm was used for high-luminosity production at 6.5 TeV in run 2 [2], while a β^* in the range of 50–100 m (reported in Table I) was used for this special physics run at 450 GeV.

The physics motivations of this run were the measurement of the elastic cross section and the extrapolation of its

TABLE I. LHC operational parameters during the high-β^* physics run at 450 GeV in October 2018.

IP	β^* Beam 1 (m) (plane)	β^* Beam 2 (m) (plane)	Crossing angle (μrad) (plane)	Separation (mm) (plane)
1	53 (H), 98 (V)	53 (H), 101 (V)	0	0
2	10 (H), 10 (V)	10 (H), 10 (V)	170 (V)	3.5 (H)
5	76 (H), 97 (V)	63 (H), 95 (V)	0	0
8	10 (H), 10 (V)	10 (H), 10 (V)	−170 (H)	−3.5 (V)

FIG. 1. Illustrative layout of the ALFA and TOTEM stations around IP1 and IP5, respectively, used in this high-β^* physics run at $\sqrt{s} = 900$ GeV.

nuclear part to the four-momentum transfer squared $t = 0$, together with the evaluation of the real-to-imaginary ratio of the forward hadronic amplitude (i.e., the ρ parameter) by accessing the Coulomb-nuclear interference region [3].

The smaller the $|t|$, the smaller the scattering angle, and the closer the trajectory of the elastically scattered proton will be to the circulating beam envelope. Thus, dedicated detectors housed in movable Roman pots (XRPs) and transversally placed very close to the edge of the circulating beam are used for this data taking.

A recent determination of the ρ parameter at $\sqrt{s} = 13$ TeV revealed values significantly lower than predicted by many theoretical and phenomenological models that typically neglect the crossing-odd t-channel exchange of colorless three-gluon compound states [3]. On the other hand, there are models that take the crossing-odd exchanges into account and are in agreement with total cross-section measurements at various energies and the ρ value at $\sqrt{s} = 13$ TeV. However, these models give different predictions for the ρ parameter at lower energies. This motivates the specific setup of the LHC that provides collision at $\sqrt{s} = 900$ GeV, in order to collect a data set that could allow one to discriminate between models that try to explain these recent results [3].

The preparation of this run poses several challenges from the accelerator physics point of view, requiring the design of dedicated beam optics [4] and collimation layouts and settings [5], to allow probing values of t as small as possible. On the other hand, machine-protection constraints are relaxed with respect to standard physics operations, given the very low circulating intensity and beam energy needed. One of the main limitations of a conventional collimation approach is the induced background on XRPs, which is linked to its intrinsic nature. Multiple Coulomb scattering in amorphous collimators is used to increase the transverse particle amplitude in a standard multiturn cleaning process, while the use of bent crystals as a primary collimation stage promises a faster cleaning process and reduced multiturn halo population. Thus, the relaxed machine-protection constraints, combined with the peculiar needs of this special physics run, provide the ideal conditions for the operational deployment of crystal collimation in the LHC. Crystal collimation was already used
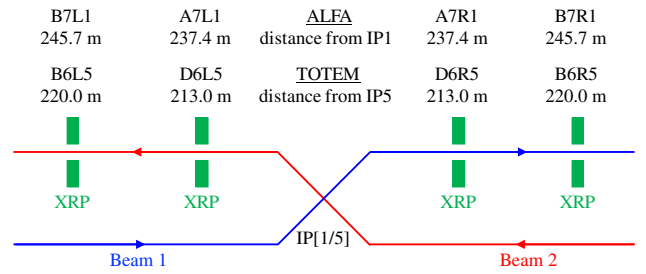
in some Tevatron collider stores in the 2010's, showing a twofold reduction of beam losses in detector regions [6,7]. However, this technique was not regularly used after. The added value of the results in this paper is showing that a reduction by more than a factor 10 of beam-related experimental backgrounds is achievable using crystals, while their operation does not cause any overhead thanks to the significant technological improvements made along the years.

The detectors used for forward physics experiments are based on tracking detectors housed in XRPs and designed to reconstruct tracks of forward protons emerging from elastic and diffractive scattering events at the interaction point (IP). The XRPs consist of movable stations where the detector is placed inside a secondary vacuum vessel, called pot, which is transversally moved into the primary vacuum of the machine [8]. Two sets of XRP stations are installed on the outgoing beams downstream of IP1 and IP5, which are operated by the ATLAS (ALFA) [9] and TOTEM [10] collaborations, respectively. Different XRPs with dedicated settings are used depending on the physics goal of the data taking. Only vertical XRP stations (each with a top and a bottom jaw) are used for this specific physics run, in total four stations for each IP, as shown in Fig. 1.

The results reported in this paper show the maturity reached by this powerful and innovative beam-manipulation technique that relies on bent crystal, of which a historical review can be found in Ref. [11]. Reference crystal positions are established prior to the physics run, during which a fully automated crystal handling is deployed. Even though this special run is much shorter than the standard physics run at the LHC, the crystal-collimation scheme shows stable performance, while a realignment of some collimators is required for the standard scheme. Moreover, the evidence of reduction of the beam-related background rate at the experiments is obtained using crystals with respect to a standard collimation approach. The solid operational and experimental performance obtained, enhance the possibility to use bent crystals in future applications at high-energy colliders that

may be required by the high-energy physics community, as also presently under investigation in the framework of Physics Beyond Colliders studies at CERN [12–14].

An introduction to the LHC collimation system is given in Sec. II, while the main challenges and possible applications of bent crystals are reported in Sec. III. Studies performed in preparation of the high-β^* physics run are reported in Sec. IV. An overview of the operational procedures used during the data taking is reported in Sec. V. The experimental results are discussed in Secs. VI and VII, together with a comparison with theoretical expectations. An explanation of the background asymmetry observed between beams is given in Sec. VIII. All abbreviations used in the text are summarized in Appendix A, and the complete list of collimator settings is provided in Appendix B.

II. THE LHC COLLIMATION SYSTEM

The LHC demands a tight control of beam loss because of its cryogenic nature. Tens of mJ/cm^3 deposited in superconducting magnets by hadronic showers developed from circulating protons that are lost on them, can cause an abrupt loss of their superconducting properties, i.e., a magnet quench. On the other hand, more than 300 MJ were stored in the LHC circulating beams during run 2 [15]. Thus, a highly efficient collimation system is required in order to minimize the amount of deposited energy in the superconducting magnets by beam loss.

An illustrative picture of the working principle of the LHC collimation system is given in Fig. 2(a). The present LHC system [16–19] is composed of 44 movable ring collimators per beam, placed in a precise multistage hierarchy
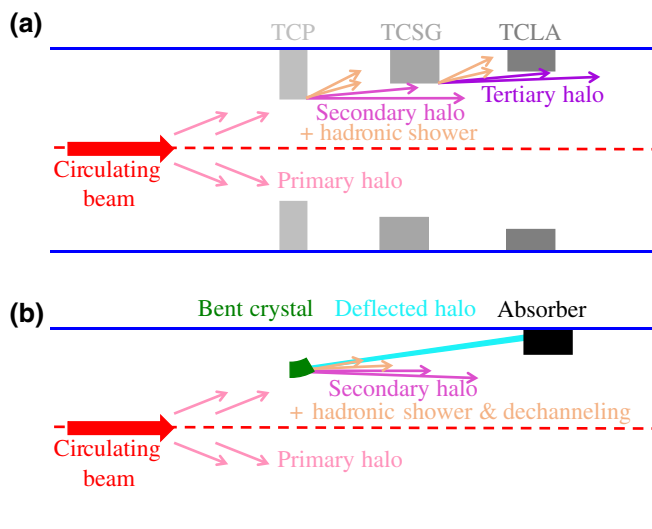
of gaps that must be maintained in any machine configuration to ensure optimal cleaning performance. Two LHC insertion regions (IRs) are dedicated to beam-halo collimation: IR3 for momentum cleaning, i.e., removal of particles with a large energy offset; and IR7 for betatron cleaning, i.e., controlled disposal of transverse halo particles. Each collimation insertion features a three-stage cleaning based on primary collimators (TCPs), secondary collimators (TCSGs), and absorbers (TCLAs). In this scheme, the energy carried by the beam halo intercepted by TCPs is distributed over several collimators (e.g., 19 collimators are installed in the betatron cleaning insertion per beam). Dedicated collimators for protection of sensitive equipment (such as TCTPs for the inner triplets that are the last three quadrupoles before the interaction point, which represent the physical aperture bottleneck during standard physics data taking), absorption of physics debris (TCLs) and beam injection and dump protection (TDIs-TCLIs and TCDQs-TCSPs) are also present at specific locations of the ring. All collimators consist of two movable blocks (except the single-sided dump protection block TCDQ), called jaws, that are centered around the circulating beam. A detailed description of these functionalities goes beyond the scope of this paper and can be found in Ref. [16]. The complete collimation layout of the LHC as of run 2 is shown in Fig. 3.

The standard collimation scheme is routinely used in normal operations. In addition, a crystal-collimation test stand is installed in IR7 [20] allowing experiments with

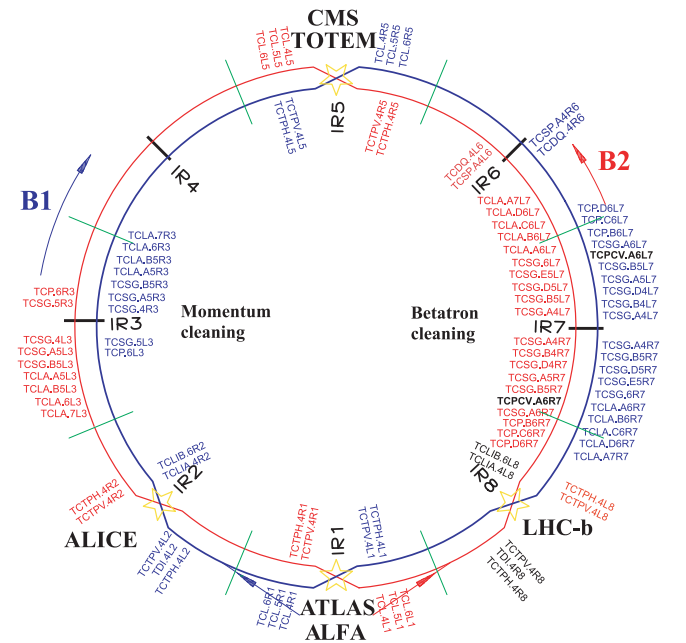FIG. 2. Working principle of the (a) standard and (b) crystal-collimation system in IR7.

FIG. 3. Collimation layout in the LHC as of run 2. The two counterrotating beams are indicated as B1 and B2 and shown in blue and red, respectively. Names and functionality of each collimator are specified in Appendix A.
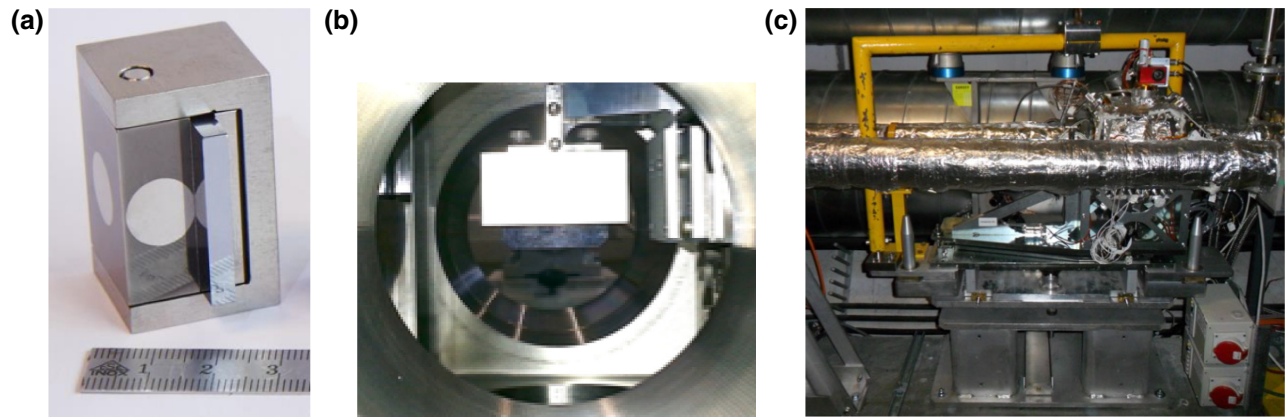
FIG. 4.   Pictures of the crystal (a) in its holder, (b) as seen by beam 1 when installed in the goniometer, and (c) of the full assembly TCPC.A6L7 installed in the LHC tunnel (on beam 1 that is on the external beam pipe in IR7, see Fig. 3).

this innovative collimation technique to be performed. An illustrative picture of the working principle of a crystal-collimation system is given in Fig. 2(b). The main difference with respect to the standard approach is that primary collimators are replaced with bent crystals. Halo particles are intercepted by a 4-mm-long crystal with a bending of 50 μrad that coherently deflects them onto a single absorber by means of crystal channeling, as opposed to the standard approach, where 60-cm-long jaws of carbon-fiber composite are used. The kick given to a 7-TeV proton by such a crystal is equivalent to that of a magnetic field of about 310 T ideally acting only on a selected beam portion. A total of four crystals are installed in IR7, two per beam and one per plane. Details about the layout design and crystal characteristics are reported in Ref. [20], which allows the first observation of crystal channeling with 6.5-TeV proton beams [21]. The two quasimosaic crystals [22] acting on the vertical plane, provided by the UA9 collaboration and built at the Petersburg Nuclear Physics Institute (PNPI), are used in this specific physics run. An illustrative picture of the vertical crystal installed in beam 1 is given in Fig. 4(a), where two round mirrors engraved on the holder can be seen. These are instrumental to align the crystal during the installation in the goniometers. A picture of the fully inserted crystal as seen by beam 1 is shown in Fig. 4(b), while the complete goniometer assembly after the installation in the LHC tunnel is reported in Fig. 4(c). Extensive crystal-collimation studies are performed throughout run 2 of the LHC, which demonstrates reliable channeling along the entire cycle of the machine [23].

III. MAIN CHALLENGES AND POSSIBLE APPLICATIONS OF BENT CRYSTALS

The LHC crystal are made of silicon produced with high purity lattice and dislocations below $1/cm^2$. Present cutting and bending techniques provide crystals essentially

without amorphous layer facing the beam and with uniform bending [22,24], which significantly improves the performance for usage in circular colliders. The single-pass channeling efficiency is typically in the range of 60%–70% [25], while a multiturn channeling efficiency up to 90% is obtained in circular machines [26].

One of the most challenging operational requirements is the angular alignment of the crystalline planes with respect to the beam envelope. The channeling acceptance at LHC energies diminishes from about 9.5 μrad at 450 GeV to about 2.5 μrad at 7 TeV. A high-resolution goniometer is developed, featuring a piezo actuator and a stepper motor for the rotational and linear stages, respectively. The same high-performance motors with 5-μm resolution as developed for the LHC collimators are used for the linear movement. The piezo actuator provides an angular resolution below 0.1 μrad and a stability below 1 μrad also during the execution of combined linear and angular time functions required to follow the beam envelope during the energy ramp [27,28]. This hardware represents a significant technological step that makes it possible to operate crystals as efficiently as any other collimator throughout the entire machine cycle.

Crystal aging, mainly due to ionization losses and inelastic interactions, is not expected to be problematic. Particles channeled between crystalline planes generate only half as much ionization as in amorphous materials, and the crystals are so small that hadronic showers will develop outside their volume. Studies to assess the channeling performance as a function of the radiation dose are ongoing, and present estimates show that crystals can operate with high-intensity LHC beams for several years without showing any performance degradation [29]. The crystals do not show signs of damage from beam impacts equivalent to the worst LHC accident scenario [30].

Presently, the main challenge left to make crystal collimation operational with high-energy and high-intensity proton beams (about 300-MJ stored energy at the LHC,

which will become about 700 MJ at HL-LHC) is the safe disposal of channeled halo particles in accident scenario. With an expected beam-loss power up to 1 MW at HL-LHC, of which a large fraction would be deposited on a surface of few mm^2, a traditional LHC collimator will not be able to safely absorb this load. This aspect and the fact that the leakage of energy out of this absorber must be minimal in order to avoid quenches of downstream superconducting magnets, pose obvious challenges for the design of channeled halo absorption. Preliminary studies for the LHC indicated that this solution is not feasible for practical purposes without a major redesign of the betatron collimation layout. Crystal collimation of high-intensity proton beams is therefore not presently pursued for the LHC upgrade. The situation changes drastically for HL-LHC heavy-ion beams, where a 20-MJ stored beam energy causes a power load of up to a few kW [31] on the traditional LHC collimator used to absorb channeled ions.

For heavy-ion operation, the impedance of the crystal assembly is well within the accepted range and no issues are expected regarding both beam stability and local heating [32].

The crystals were also tested as primary collimators during several heavy-ion fills in 2018 with up to 4 MJ of stored energy over a few hours [33,34], and have recently been included in the HL-LHC baseline [35].

Other applications of bent crystals under study at CERN are their use to allow fixed-target experiments in the LHC primary vacuum without the need of a dedicated extraction line [14] and shadowing of the SPS septum to reduce slow extraction beam loss [36]. A feasibility study to prove the concept of local nonresonant beam extraction from the LHC was also proposed [37].

Moreover, crystals are highly versatile tools that have been used for a large variety of purposes and are under investigation in various laboratories for new innovative applications. In the domain of high-energy physics, crystal diffraction allowed to reach the best estimates of K$^{\pm}$ meson and Σ^- baryon mass [38–40]. The use of crystals for high-energy beam manipulations include also beam focusing and mirroring [41–44], with potential applications for collimation, cooling, and steering of secondary particle beams [45,46]. Proposals for production and acceleration of future muon beams are under study [7,47,48]. At lower beam energies, interesting developments are ongoing for the use of crystals as ondulators for the next generation of intensive γ-ray light sources by means of channeling of electrons and positrons [49–55]. Applications to astrophysics are also under discussion, such as the use of crystals for Laue lensing [56] and high-energy spectrometers [57,58]. Last but not least, medical applications can be envisaged, such as the possibility to increase the yield of radioisotope production by enhancing the inelastic nuclear interaction probability [59–61], and the first conceptual studies to replace gantries for dose delivery in hadron therapy are ongoing [62].

IV. HIGH-β^* PHYSICS RUN PREPARATION

The preparation of the high-β^* run at 450 GeV posed several challenges from the machine point of view [4]. In particular, dedicated optics and collimator settings were conceived to allow a successful data taking. The main optics parameters and settings of the entire collimation system are reported in Tables I and II, respectively.

The LHC collimation system is normally used to safely dispose of halo particles that would be otherwise lost in superconducting magnets. On the other hand, a completely different functionality was required for this special physics run, namely mitigate the background rate on XRPs due to beam halo. Initial tests using a single-stage collimation, as used in previous high-β^* runs, showed an experimental background at both ALFA and TOTEM that was orders of magnitude too high [63,64]. Based on further studies, a two-stage collimation scheme was proposed, which was shown to give an acceptable background [5]. In the following, this is called the *standard system*. This system is based on tungsten collimators (i.e., TCLAs and TCTPs) deployed in a two-stage collimation hierarchy, featuring the tightest operational margins ever used in the LHC. Tungsten collimators are chosen because of their higher absorption efficiency compared to all other ring collimators. A retraction of 0.2σ is used between the primary and secondary collimation stage, with XRPs positioned at 0.3σ larger aperture from the secondary stage, where σ is the RMS beam size, assuming a Gaussian-beam distribution and normalized emittance $\varepsilon^* = 3.5$ μm.

The crystal-collimation scheme is developed in parallel as an alternative way to achieve possibly even lower backgrounds.

A. Definition of operational settings for crystal collimation

The settings used for standard collimation are taken as initial conditions to define settings of the crystal-collimation scheme, but using a bent crystal as the primary collimation stage. Settings are optimized to relax margins on collimation hierarchy while improving the performance. This is because both systems would be very sensitive to even small orbit drifts that risk breaking the collimation hierarchy and causing a large increase in the background of XRPs, with only a 0.2σ margin between stages.

Semianalytical tools are developed to evaluate if the channeled beam can be intercepted by the downstream collimators in these extreme conditions. The trajectory of particles experiencing an angular kick θ at the longitudinal position s_1 can be described using the transfer matrix formalism. Assuming $x'(s_1) \approx 0$ and $\alpha_1 \approx 0$, the trajectory of
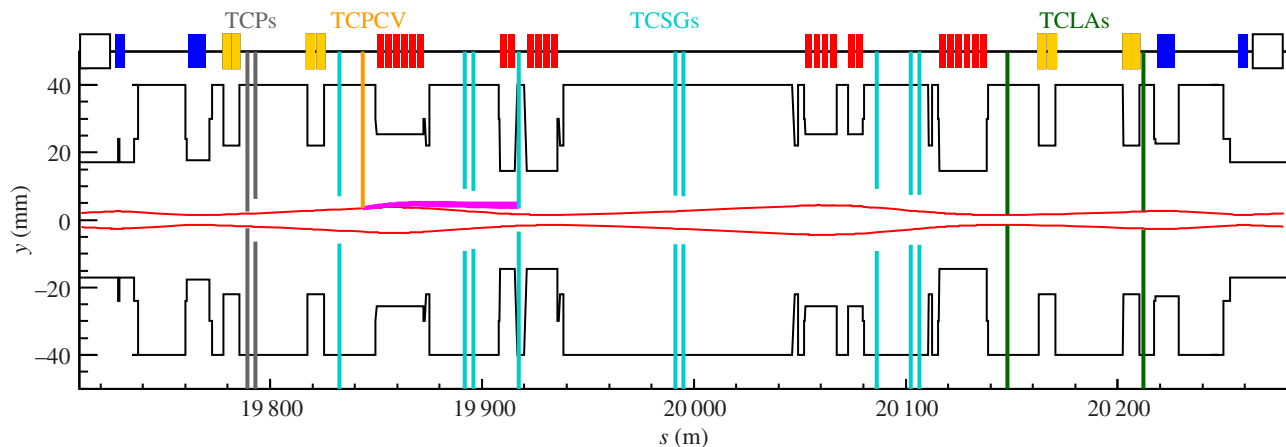
FIG. 5. Projection on the vertical plane of the trajectories of channeled halo particles and mechanical aperture of the beam pipe (black) versus longitudinal position along the IR7 insertion (in the direction of beam 1). The TCPs (gray), crystal (orange), TCSGs (cyan), and TCLAs (green) sit at apertures listed in Table II. The beam envelope at 2.5 σ is shown by the red lines, while the trajectories followed by halo particles that undergo channeling are enclosed between the magenta lines. The magnetic lattice is also drawn on the top, where blue and white boxes represent the main superconducting quadrupoles and dipoles, respectively, while normal conducting quadrupoles and dipoles are depicted by the red and yellow boxes, respectively.

a kicked particle is described by

$$x(s) = \sqrt{\frac{\beta(s)}{\beta(s_1)}} \cos\left(\Delta\mu_{s-s_1}\right) x(s_1)$$
$$+ \theta\sqrt{\beta(s)\beta(s_1)} \sin\left(\Delta\mu_{s-s_1}\right), \qquad (1)$$

where α, β, and $\Delta\mu$ are the Twiss parameters and betatron phase advance, respectively. An example of studies based on this approach is shown in Fig. 5.

The semianalytic studies are used to identify suitable collimator settings. The final layout is validated by complete multiturn tracking simulations that provided a quantitative evaluation of the expected background at the XRPs. These simulations are performed using SixTrack [65–68] that allows a symplectic, fully chromatic, and 6D [i.e., $(x, x', y, y', E, \varphi)$, where (x, x', y, y') and (E, φ) are the coordinates in transverse and longitudinal plane, respectively] tracking along the magnetic lattice of the LHC, taking into account interactions with the ring collimators and XRPs, and the detailed aperture model of the entire machine. SixTrack has been successfully benchmarked with LHC data in Refs. [18,69,70]. The treatment of interactions between protons and bent crystals is carried out using a dedicated routine implemented in SixTrack. The details of this implementation and the physics models used can be found in Refs. [71–73], while its benchmarking in the energy range from 180 GeV to 6.5 TeV is reported in Refs. [72,74–77]. This simulation setup allows estimation of the density of protons lost per meter with a resolution of 10 cm along the entire ring circumference. The settings for both systems are reported in Table II. Note that in the crystal-based system:

(a) TCTPs in IR2 and IR8 in both beams are opened from 2.7σ to 13σ.

(b) TCTPs in IR5 of beam 1 and in IR1 of beam 2 are opened from 2.7σ to 13σ.

A significant reduction of losses on cold elements around the entire ring when using crystals instead of the standard collimation approach is expected. Nevertheless, losses on cold magnets are not the main concern for this special physics run, given the very low stored energy (< 30 kJ) compared to the standard high-intensity physics runs (>300 MJ). The main focus is the number of impacts on XRPs for a given collimation scheme, as further discussed in Sec. VI.

V. HIGH-β^* PHYSICS RUN OPERATIONS

Promising results are obtained with both collimation schemes during initial tests on the 2 October 2018 (Fill 7249). Thus, it is decided to keep the crystals as a viable option for the physics run.

A. Operational procedures

The physics data taking is carried out from 11 to 13 October 2018, with 450 GeV proton beams circulating in the machine. The overview of the physics fills performed is shown in Fig. 6. Two fills, one using standard (Fill 7280) and one using crystal (Fill 7281) collimation schemes, are performed after a first setup fill required to validate the results obtained in initial tests. After these two fills, a strong preference for the standard system is expressed by ALFA, while TOTEM had better results using crystals but is also satisfied with the data quality obtained with the
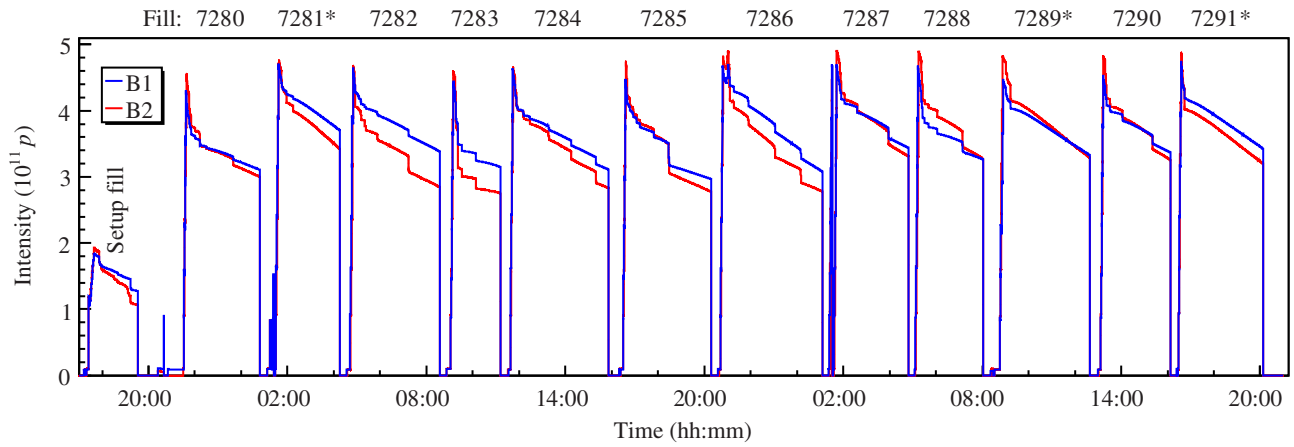
FIG. 6. Circulating beam intensity in fills performed during the high-β^* run from 11 to 13 October 2018. Fills where crystal collimation was used are marked by *.

standard system. Thus, it is decided to continue with the standard scheme for the next fills. After four fills (from Fill 7282 to Fill 7285) it is required to recenter some of the collimators to keep the required 0.2σ margin between the primary and secondary collimation stage. Unfortunately, the TOTEM data quality is significantly worsened in the following three fills (from Fill 7286 to Fill 7288). Thus, crystal collimation is used for the next fills (Fills 7289 and 7291), interleaved by a fill dedicated to ALFA using the standard system (Fill 7290). A total of nine and three fills are performed using standard and crystal-collimation schemes, respectively.

An example of two fills using the different collimation schemes is shown in Fig. 7. The operational procedure followed for both collimation schemes is as follows:

1. Six bunches are injected in the machine with colli-mators at nominal injection settings reported in Table II.
2. Beams are scraped using TCP.D6[L/R]7.B[1/2] from 5.7σ to 2.5σ, with the rest of the collimation system at injection settings.
3. The entire collimation system is moved to settings reported in Table II, depending on the collimation scheme used.
4. Beams are scraped with TCLA.A6[L/R]7.B[1/2] from 2.5σ to 2.0σ.
5. TCLA.A6[L/R]7.B[1/2] are moved back to
(a) 2.5σ in the case of the standard system.
(b) 2.7σ in the case of the crystal scheme.
6. XRPs are closed to physics settings reported in Table II.

An increasing background as a function of time is observed during the fill (see Sec. VI), in particular with the standard collimation system. Thus, rescraping is per-formed on the experiments' request, i.e., when the back-ground rate is reaching values that could jeopardize the

measurement. The operational procedure followed is as below.

1. ALFA pots are retracted due to concerns for radia-tion to electronics, while this does not concern TOTEM, so those pots are left in place.
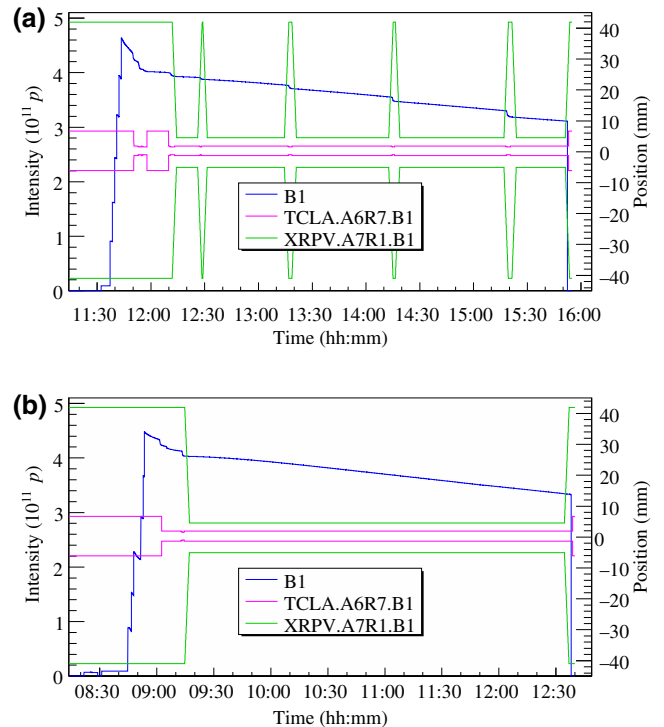

FIG. 7. Overview of (a) Fill 7284 using the standard colli-mation system and (b) Fill 7289 using the crystal-collimation system. Circulating intensity and devices only of beam 1 are shown, where TCLA and XRPV are the positions of the collima-tor used for scraping (and as primary stage in the case of standard collimation) and an ALFA Roman pot, respectively.

2. Beams are scraped with TCLA.A6[L/R]7.B[1/2] from 2.5σ to 2.0σ.

3. TCLA.A6[L/R]7.B[1/2] are moved back to 2.5σ.

4. ALFA pots are closed again to physics settings.

The main difference between the two collimation schemes is that rescrapings are not needed when using crystals, as shown in Fig. 7. The present interpretation of this feature is discussed in Sec. VI A. Thus, one of the main gains using crystals is a more efficient data taking. About one rescraping every hour is required when using the standard system. The retraction and insertion of ALFA pots required about 6 min, as shown in Fig. 7(a). Thus, about 10% less integrated luminosity is collected when using the standard system with respect to a fill of the same length in which crystal collimation is used.

B. Operational performance

The crystals need to be aligned to the circulating beam in both position and angle to achieve an optimal channeling performance. The reference position and angular orientations of crystals are defined during a setup fill on 2 October 2018. The entire alignment requires less than 25 min. The beams are approached in steps and touched at 48–49 mm from the crystal garage position (i.e., completely retracted from the nominal beam position at 0 mm), as opposed to double-sided movable objects that have the "0" in the geometrical center of the beam pipe (see also Fig. 7). Then, the crystals' angle is adjusted to find the optimal orientation of crystalline planes with respect to the beam envelope, which maximizes the channeling performance. These reference positions are used to insert the crystals directly in channeling orientation through automated sequences, used to operate the LHC during the physics run. Nevertheless, a quick check of the correct crystal positioning is performed in the shadow of the XRP insertion. An example of crystal insertion during the physics run is shown in Fig. 8. The initial loss spike shows that the halo of the circulating beam is touched when inserting the crystal. Then, the reduction of losses at the absorber used to intercept the
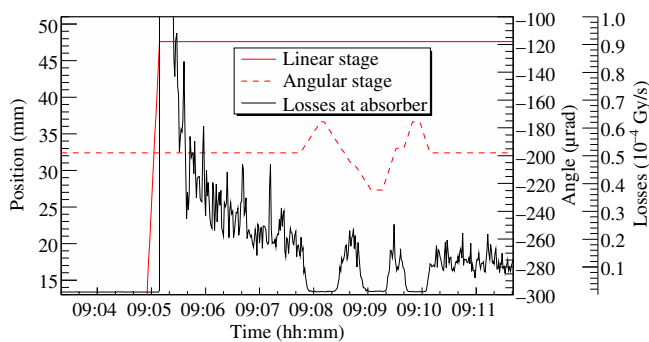

FIG. 8. Overview of the automatic insertion in channeling orientation and preliminary checks of the crystal in beam 2.

channeled halo particles when the crystal is rotated proves that crystals are actually inserted directly in channeling orientation. This check is performed in all fills in which crystals are used, showing consistent results and demonstrating reliable channeling performance along the entire run.

This operational performance is a very useful milestone, showing that crystals can be used as efficiently as standard collimators in collider operation.

VI. BACKGROUND RATES

Noncolliding bunches are injected in two fills to provide an absolute evaluation of the beam-related background rates (Fill 7284 and 7289 with standard and crystal collimation, respectively). Colliding bunches are not considered because it would be impossible to distinguish between beam-related background and physics background from the collisions.

The Beam Loss Monitor (BLM) [79] system of the LHC is not sensitive enough to detect hadronic showers generated by the interaction of the beam halo with the XRPs, because of the very low beam intensity at injection energy. Therefore, data provided by ALFA and TOTEM are used, which have a much greater sensitivity to the halo than the machine instrumentation and make it possible a direct comparison between simulations and background data.

The background rate at TOTEM is defined as the rate of events related to noncolliding bunches to which a single track is associated. No further selection is applied and the rates are corrected for the prescale factor imposed by the trigger system. Experimental data are shown in Fig. 9(a), where events recorded in time bins of $\Delta t \sim 300$ s are reported as a function of time. ALFA detectors are equipped with scintillator tiles for triggering, which are made of 3-mm-thick standard plastic scintillators [9], and raw trigger rates are provided rather than the rate of reconstructed single tracks as done by TOTEM. Thus, the trigger rate from noncolliding bunches is averaged over a time window of 300 s in order to have data points comparable to what is provided by TOTEM, as shown in Fig. 9(b).

Rates from the top and bottom pots are summed and normalized to the protons lost from the noncolliding bunches in each time bin, in order to provide suitable data for comparisons with respect to SixTrack simulations. Protons lost from the noncolliding bunches are evaluated using Fast-Beam Current Transformers (FBCTs) [80] that provide bunch-by-bunch intensity measurements. A significant asymmetry between rates measured in the two beams is present, in particular when using the standard system. This is due to the asymmetric location of XRPs with respect to the collimation system and it is correlated with the amount of material shadowing the XRPs, as discussed in Sec. VIII.
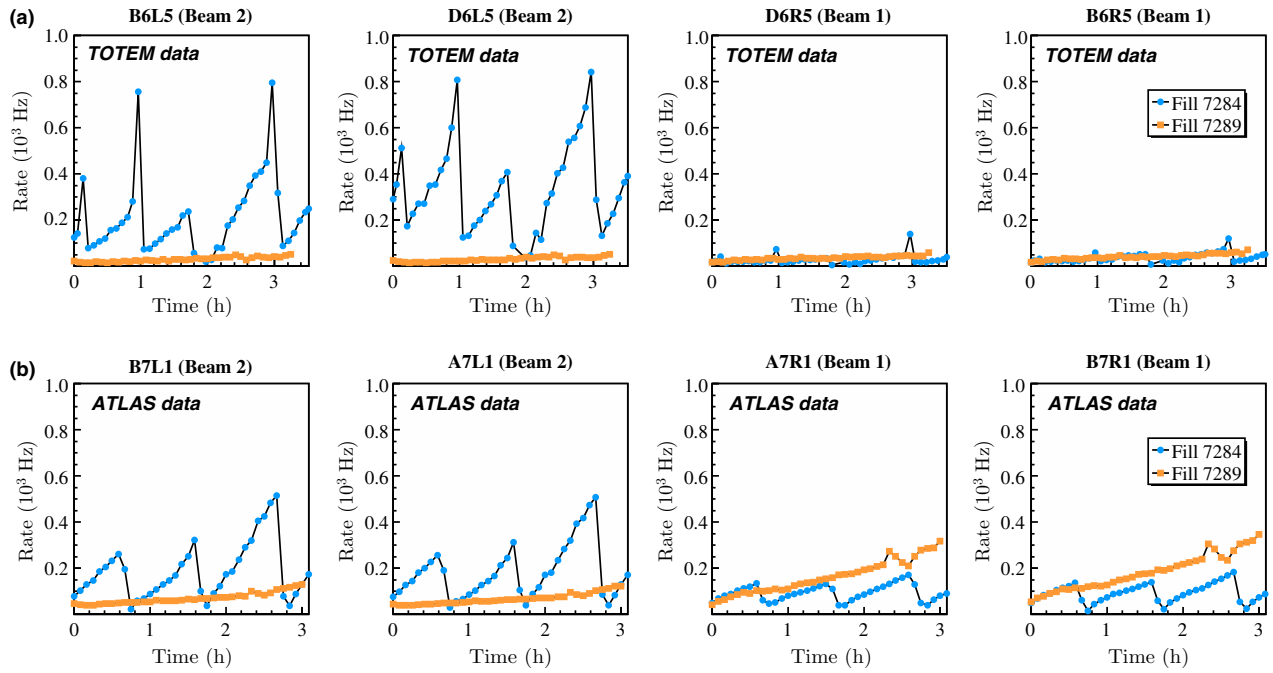
FIG. 9. Measured background rate at (a) TOTEM [78] and (b) ALFA [63] pots, using standard and crystal collimation in Fill 7284 and 7289, respectively. The rates from the top and bottom pots are added together and shown as a function of time starting from the beginning of the data taking in the different fills.

About once per hour a rescraping is needed when using the standard collimation system because of the increasing background rate, while this is not needed when using crystals, as mentioned previously and clearly visible from Fig. 9. The fill in which standard collimation is used (7284) is divided into four slices enclosed between rescrapings. The gain obtained with crystals is evaluated by dividing the counts in each time bin using standard and crystal collimation that have the same time delay relative to the retraction of the TCLA.A6[L/R]7.B[1/2] used to scrape the beam. The average ratio is compared to what is predicted by Six-Track simulations in Fig. 10. The experimental error bars represent the RMS of the measured ratio, in order to take into account systematics due to time dependence that are

not considered in simulations. A very good qualitative and quantitative agreement is obtained, as the predictions for each XRP are within experimental error bars. The simulated background ratio rate at the eight XRP stations is obtained by scoring the number of hits in the detector's active area, normalized to the total number of protons intercepted by the given collimation scheme. Then, impacts expected using the standard system are divided by the ones expected using crystals.

A. Discussion on background-rate improvement

Investigations are carried out to understand why the background rates obtained with crystal collimation are much more stable than with the standard system, without requiring any rescraping within a fill.

Let us define the multiturn halo as the particles that are not absorbed after the first impact on a collimator and keep circulating in the machine. The background rate is directly linked to the amount of multiturn halo, i.e., the more populated the multiturn halo, the larger the background rate. The multiturn halo increases if the speed with which particles diffuse into the collimation system, is larger than the speed with which they are removed. Thus, the working hypothesis is that bent crystals provide a faster halo removal. Moreover, all particles out scattered from standard collimators will populate the multiturn halo, while only particles that are not channeled for the entire crystal length may contribute to it. This makes the system able
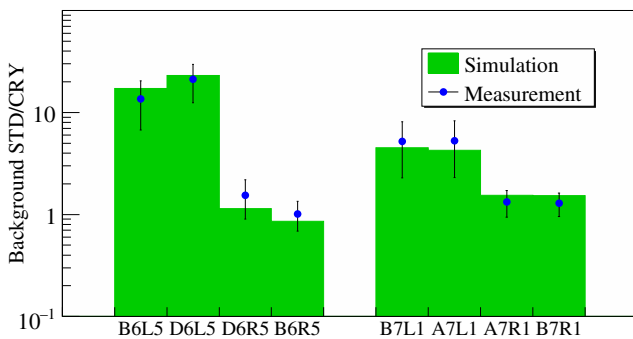

FIG. 10. Comparison between the measured and the simulated background ratio at the TOTEM and ALFA XRPs.
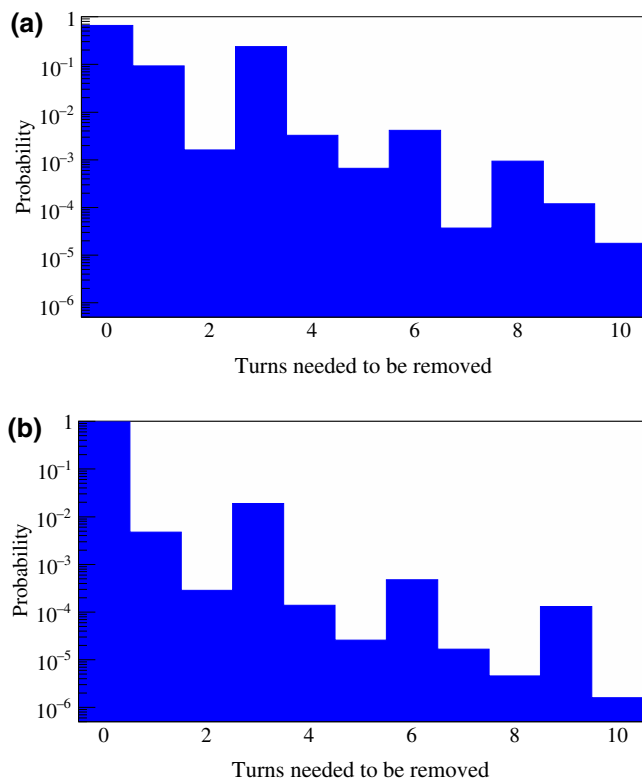
(a)

(b)

FIG. 11.   Probability of the number of turns needed for halo protons to be removed from the circulating beam after being intercepted by the primary stage using (a) standard and (b) crystal collimation.

to digest larger diffusion rates without accumulating an increasing halo population over time.

Simulations are carried out to support this hypothesis. Let us define the particle removal rate performance of the simulated system as the distribution of number of turns that particles perform between hitting the primary collimation stage and being removed from the circulating beam. The probability distribution of the number of turns needed to be absorbed is shown in Figs. 11(a) and 11(b) for the standard and crystal-collimation schemes, respectively. The studies show that 98% of the particles impacting on the crystal are absorbed within the same turn, while only 66% are absorbed in the same turn after impacting on a standard primary collimator. This means that only 2% of the particles intercepted by the bent crystals needs multiple turns to be absorbed, populating the multiturn halo and possibly contributing to the experimental background on XRPs, while this fraction increases to 34% when particles are intercepted by amorphous primary collimators. The recursive structure of a peak of absorption every three turns that is visible in Fig. 11 is due to the fractional tune of the LHC that is close to 1/3 (Vertical tune = 60.316). Thus, every particle will pass by any longitudinal location of the ring with similar transverse coordinates about every three turns.

In conclusion, this observation gives us the required confidence on the reliability of our hypothesis and that the measured background stability indicates a faster halo removal with crystals.

Similar studies could be performed on individual pots (i.e., top and bottom) as a further step, instead of summing their signal. This type of analysis could give additional information on the expected performance of a crystal-collimation system based on two crystals placed on opposite sides of each collimation plane (as opposed to the single-sided crystals presently installed in the LHC), but this goes beyond the scope of this work.

VII. BACKGROUND DISTRIBUTION

The same fills with noncolliding bunches circulating in the machine (Fill 7284 and 7289) are used for qualitative comparisons between the simulated and measured background hit pattern.

A. TOTEM Roman pots

The measured hit distributions associated to single-track events from noncolliding bunches (representing beam-related background for experiments) is shown in Fig. 12, for both collimation schemes. The simulated pattern is reported in Fig. 13, where the hits in each bin are normalized to the number of particles entered in the collimation system, showing a good qualitative agreement with respect to measurements. The D units are tilted 8° around the beam center to have multitrack resolution [81].

The improved data quality using crystals becomes clearer when also colliding bunches are taken into account [82]. In particular, structures due to multiturn halo hitting the detector edges facing the circulating beam show a similar magnitude as the physics signal, when using the standard system. On the other hand, these structures are significantly suppressed when using crystals and only the signal due to elastic scattering is clearly visible. The full offline event reconstruction, which is out of the scope of this work, clearly shows the improved data quality when using crystals [82].

B. ALFA Roman pots

The measured and simulated background distributions on ALFA XRPs are reported in Figs. 14 and 15, respectively, showing a good qualitative agreement.

Structures due to the multiturn halo hitting the detector edges facing the circulating beam are present using the standard system also in this case. On the other hand, the hit pattern using crystals is more focused on the central region of XPRs in beam 2, i.e., where the physics signal is expected. Thus, a less efficient offline background subtraction is envisioned, leading ALFA to prefer using the
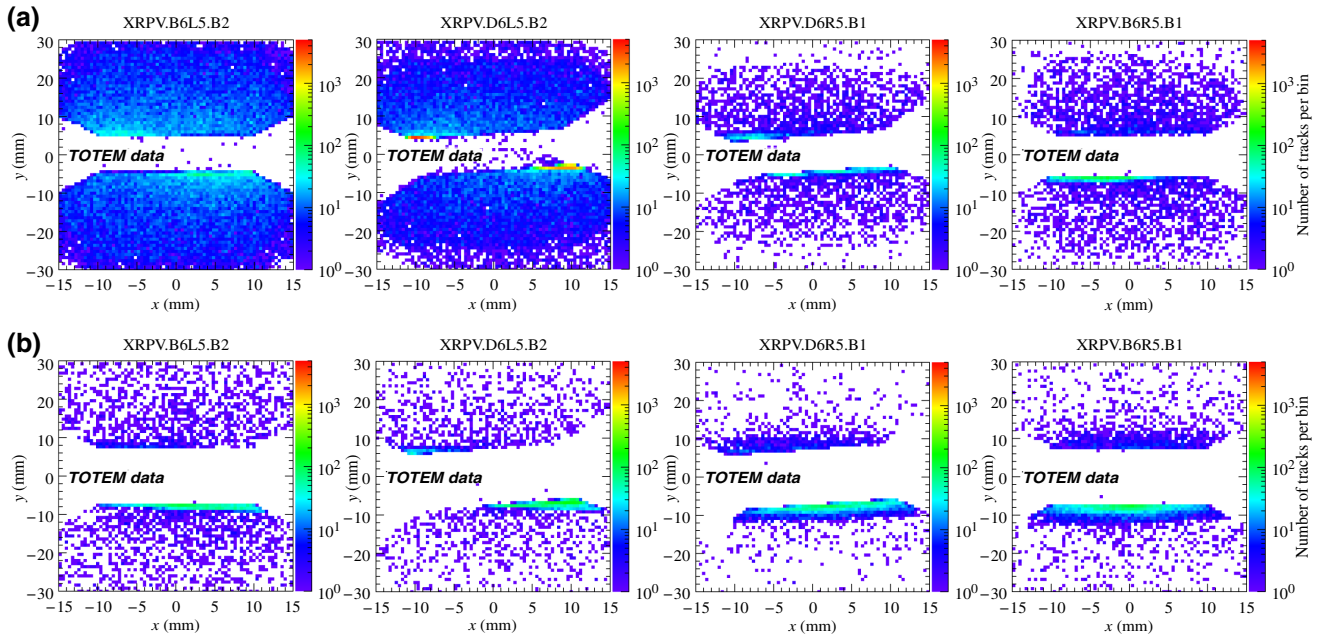
FIG. 12.   Measured background hit pattern on TOTEM Roman pots using the (a) standard and (b) crystal-collimation schemes, in Fill 7284 and 7289, respectively.

standard collimation scheme. However, full offline analysis shows that the irreducible background using standard and crystal schemes is about 0.5% and 1.5% [63], respectively. Hence, data taken using crystal collimation could be used without problems. Initially the background rate is optimized, while it later became clear that also its spatial distribution is important for ALFA. Thus, there is

not enough time to find an appropriate solution through detailed simulations while performing the run. Nevertheless, a sound explanation is found and discussed in Sec. VII C.

The screening effect of the LHC beam pipe is clearly visible in Fig. 14, causing a quite sharp drop of the number of tracks (i.e., the green area). The final output of SixTrack
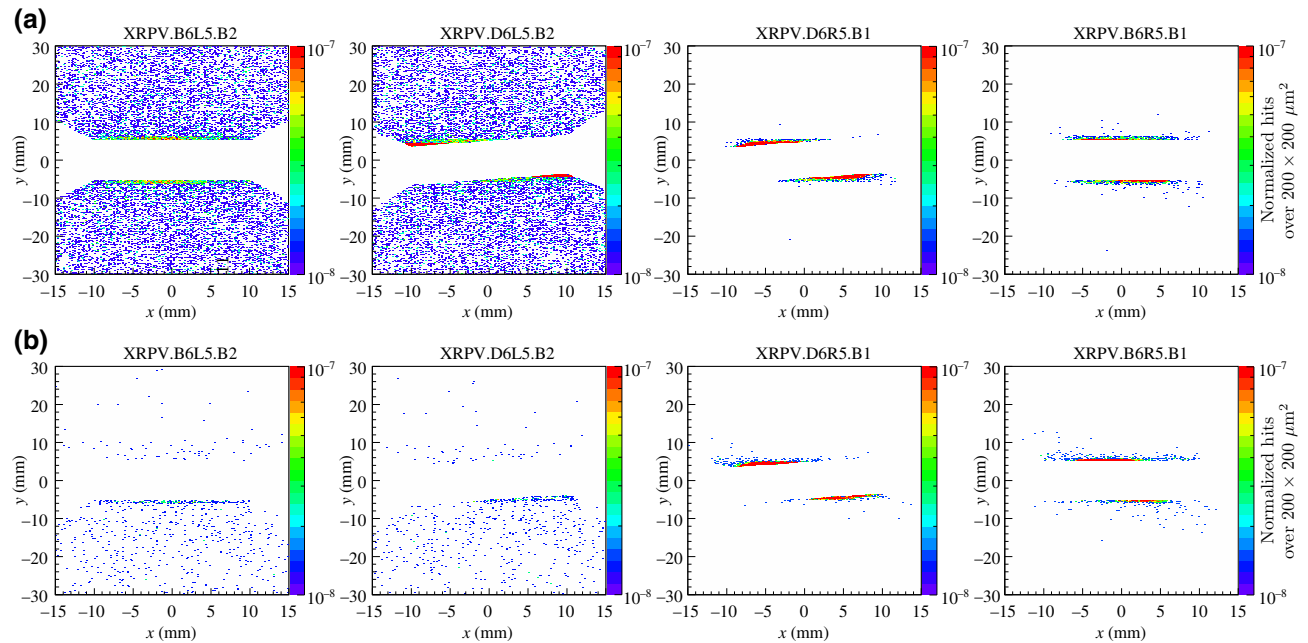

FIG. 13.   Simulated background hit pattern on TOTEM Roman pots using the (a) standard and (b) crystal-collimation schemes.
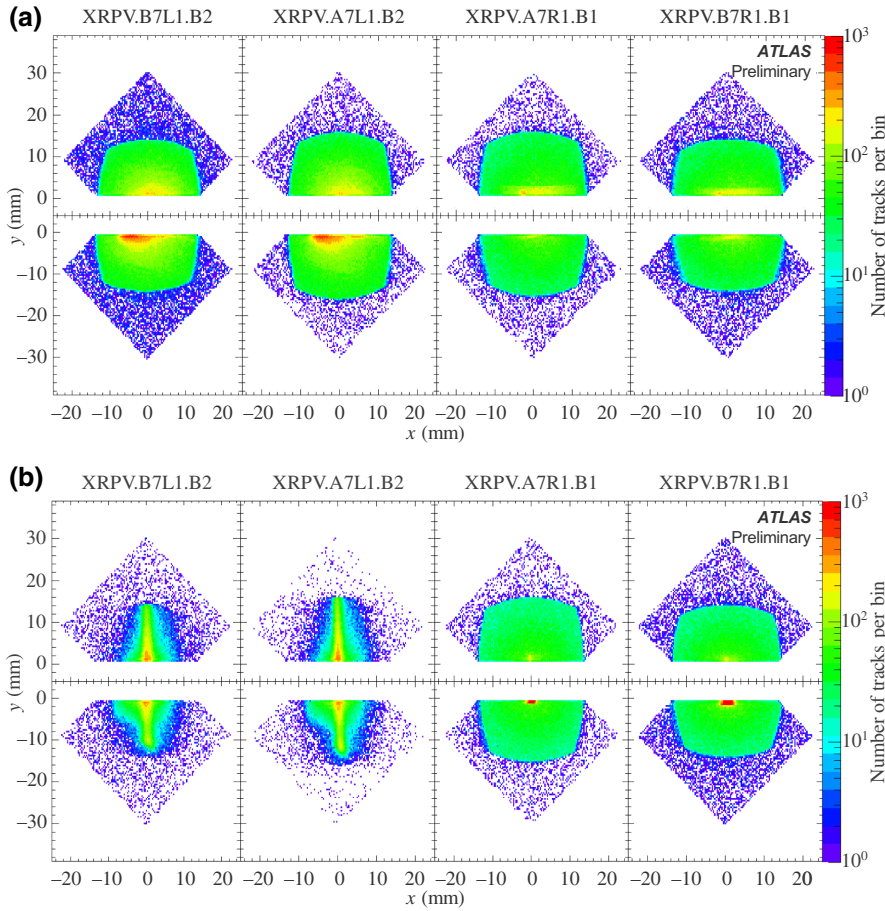
FIG. 14. Measured background hit pattern on ALFA Roman pots using the (a) standard and (b) crystal-collimation schemes [63], in Fill 7284 and 7289, respectively.

simulations is the density of protons lost on the machine aperture, as introduced in Sec. IV A. Thus, the LHC beam pipe is treated as a black absorber and its presence is not considered when producing Fig. 15 for this qualitative comparison, which otherwise would show a sharp cut [83]. This effect is not visible in Fig. 12 because TOTEM provides hits associated to the reconstructed tracks while ALFA provides all the hit map related to the raw trigger rates, as introduced in Sec. VI.

C. Understanding and correcting ALFA background distribution

A potentially problematic background distribution is observed with the crystal scheme on the ALFA XPRs in beam 2, as mentioned in Sec. VII B and shown in Fig. 14(b). Very high statistics simulations are carried out to reconstruct the pattern shown in Fig. 15(b). In particular, about 10^8 protons intercepted by the collimation system are simulated and the history of each particle reconstructed. A sketch of the mechanism generating this characteristic background structure is reported in Fig. 16.

1. A fraction of particles intercepted by the crystal in IR7 undergo dechanneling and bypass the absorber because of the reduced deflection acquired.

2. These particles circulate for tens of turns in the machine.

3. A fraction of these particles hits a TCLA in IR3 (TCLA.A5L3.B2).

4. A fraction of these particles emerges from the TCLA.A5L3.B2 and hits the ALFA XPRs in beam 2 at the same turn.

The peculiar shape of the hit pattern is mainly due to the fractional betatron phase advance from the TCLA.A5L3.B2 and ALFA XRPs in beam 2, which is as follows:

(a) $\Delta\mu_x^{\text{XRP-TCLA}} \sim 4°$;
(b) $\Delta\mu_y^{\text{XRP-TCLA}} \sim 244°$.

Moreover, the deflection due to elastic scattering (θ_{el}) acquired in the TCLA.A5L3.B2 is isotropic, but induces a different displacement at ALFA XRPs depending on optics parameters. Starting from Eq. (1) one can compute

$$\frac{\Delta y(\theta_{\text{el}})}{\Delta x(\theta_{\text{el}})} \propto \frac{\theta_{\text{el}}\sqrt{\beta_y^{\text{TCLA}}\beta_y^{\text{XRP}}}\sin(\Delta\mu_y^{\text{XRP-TCLA}})}{\theta_{\text{el}}\sqrt{\beta_x^{\text{TCLA}}\beta_x^{\text{XRP}}}\sin(\Delta\mu_x^{\text{XRP-TCLA}})} \approx 20. \quad (2)$$
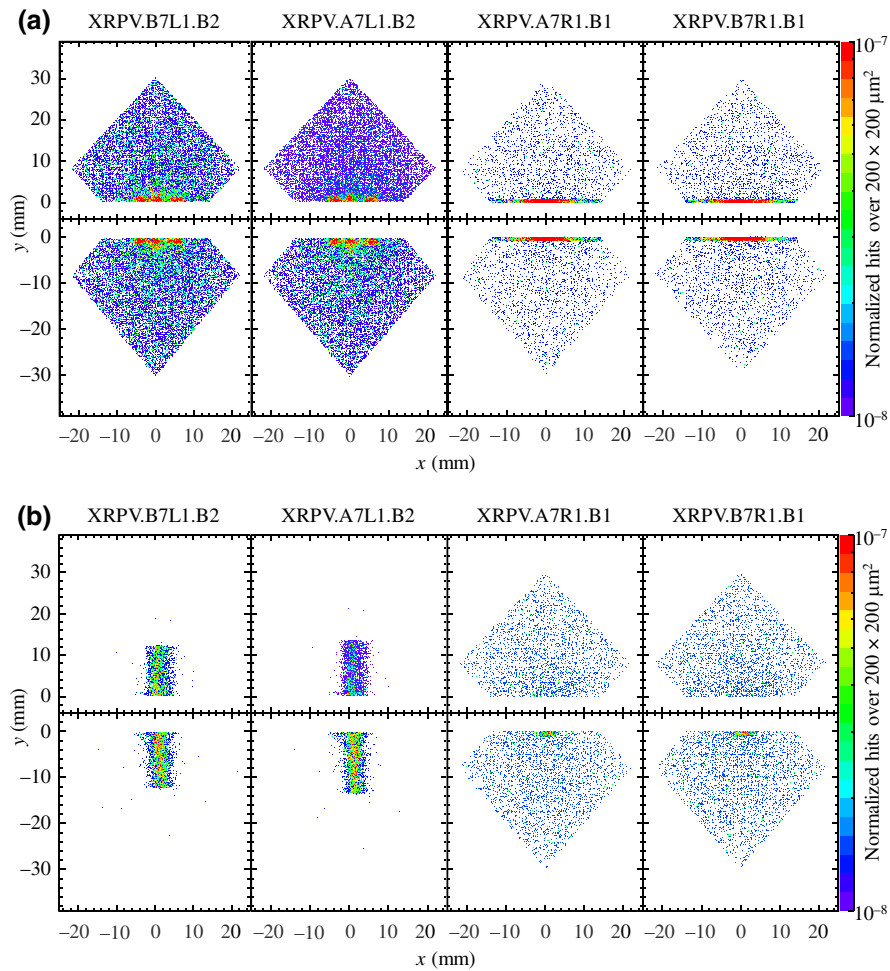
FIG. 15. Simulated background hit pattern on ALFA Roman pots using the (a) standard and (b) crystal-collimation schemes.

Thus, a kick imparted at the TCLA.A5L3.B2 induces a displacement at the ALFA XRPs in beam 2 that is about 20 times larger in y than x, leading to the characteristic pattern observed.

A cross-check is performed in simulations, placing all the system at settings reported in Table II except the TCLA.A5R3.B2 that is opened to 13 σ. The distribution obtained is reported in Fig. 17 and does not show the potentially problematic structure anymore, as expected
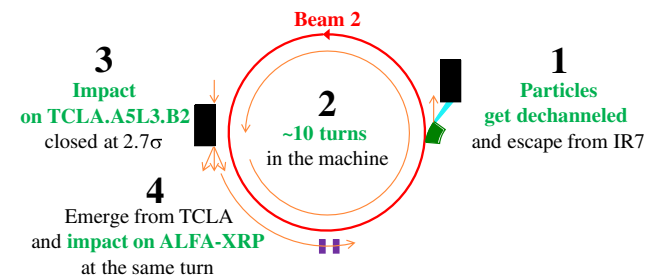

FIG. 16. Sketch of the history of particles leading to the potentially problematic background distribution on ALFA XPRs in beam 2.

after removing the identified source of background. It is noted that opening the TCLA.A5L3.B2 would have led to an even larger reduction of background rate with respect to the standard system at ALFA, while the gain would be reduced at TOTEM.

This proves that, according to numerical simulations, the potentially problematic background distribution observed by ALFA is not intrinsically related to the use of bent crystals. The good qualitative and quantitative agreement between predicted and measured background rate and distribution obtained, give us the confidence that the accuracy of the available simulation tools will make it possible to achieve even better performance if the use of crystal collimation is defined as the baseline in future runs, rather than adapting the insertion of crystals in a conventional system.

VIII. UNDERSTANDING THE BACKGROUND ASYMMETRY BETWEEN THE BEAMS

Numerical investigations are carried out to find a qualitative explanation for the observed asymmetry between the background rates in the two beams, in particular when using the standard collimation scheme. The history of each simulated particle impacting the XRPs is reconstructed
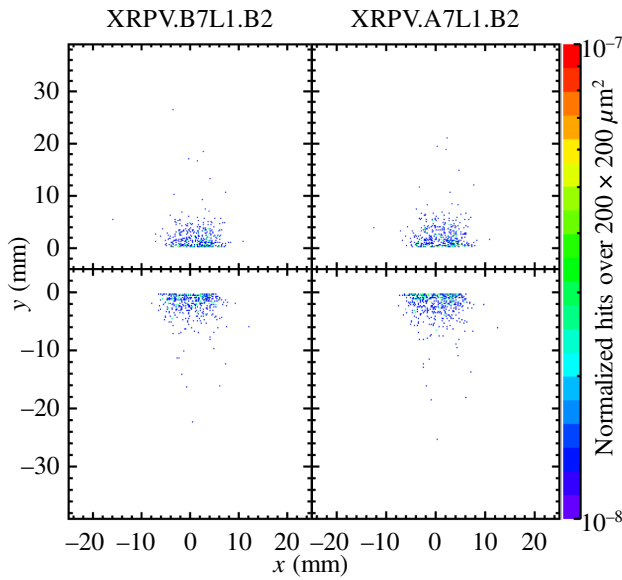
FIG. 17. Simulated background hit pattern on ALFA Roman pots in beam 2, using the crystal-collimation scheme and retracting the TCLA.A5L3.B2.

to understand the underling processes leading to beam-related background, as also discussed in Sec. VII C. Most of the hits on XRPs come from protons that emerge from the collimator used as primary stage, survive also the interaction with collimators used as secondary stage, and finally reach a XRP. All these three steps take place in the same turn. Thus, it is a single-pass process. Then, one can think that the more secondary-stage collimators are physically present between primary stage and XRPs, the fewer will be the protons able to reach the XRPs. This is true only when the betatron phase advance between the different

devices is taken into account. Thus, the phase-space coverage between the primary collimation stage and XRPs is evaluated.

An example regarding the TOTEM XRPs in beam 2 is shown in Fig. 18(a). Collimators starting from the primary stage (i.e., TCLA.A6L7.B2) to the XRPs are represented by shaded gray areas, while XRPs are drawn in cyan. Only two collimators acting as secondary stage are present (i.e., TCLA.D6L7.B2 and TCTPV.4R5.B2) that cover different phase-space regions and partially shade the XRPs. Thus, particles impacting on the XRPV.D6L5.B2 and XRPV.B6L5.B2 survive the interaction with one or two 1-m-long collimator jaws made of tungsten, after emerging from the primary stage. Moreover, the XRPV.D6L5.B2 is tilted by 8°, pushing one corner outside of the shadow of the secondary stage, as visible in Fig. 18(a). Thus, that corner is exposed to direct impact of protons that emerge from the TCLA.A6L7.B2 acquiring a deflection that is not sufficient to be intercepted by the TCLA.D6L7.B2 and TCTPV.4R5.B2, but it is enough to reach the XRPV.D6L5.B2 corner, as confirmed by the observations reported in Sec. VII A.

An example regarding the ALFA XRPs in beam 2 is shown in Fig. 18(b). The XRPs are fully shadowed by one collimator in this case, i.e., TCTPV.4R5.B2, which means that the XRPs and that collimator have the same betatron phase advance with respect to the collimator used as primary stage. Moreover, the XRPs are partially shadowed by three other collimators. Thus, protons emerging from the primary stage should survive the interaction with at least 1 m and up to 4 m of tungsten before reaching the XRPs.

In conclusion, based on the phase-space coverage between the primary collimation stage and XRPs, the ordered list of highest number of hits is as follows.
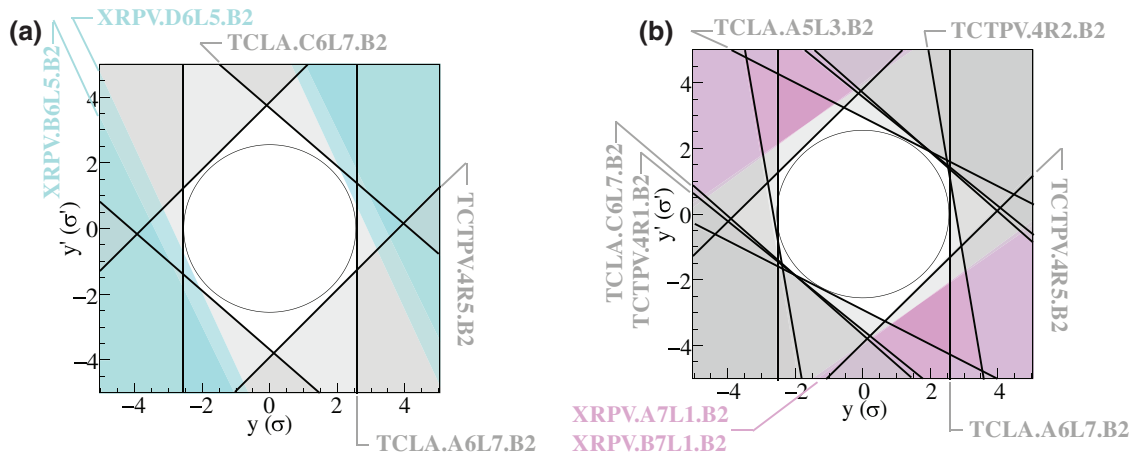

FIG. 18. Normalized phase-space coverage regarding (a) TOTEM XRPs and (b) ALFA XRPs in beam 2. Collimators starting from TCLA.A6L7.B2 to the XRPs are represented by shaded gray areas, while TOTEM XRPs and ALFA XRPs are drawn in cyan and magenta, respectively.

1. TOTEM XRPs in beam 2, because partially shadowed by two collimators, i.e., from 1 to 2 m of tungsten.
2. ALFA XRPs in beam 2, because fully shadowed by one collimator plus partial shadow of three collimators, i.e., from 1 to 4 m of tungsten.
3. ALFA XRPs in beam 1, because fully shadowed by two collimators plus partial shadow of one collimator, i.e., from 2 to 3 m of tungsten.
4. TOTEM XRPs in beam 1, because fully shadowed by three collimators plus partial shadow of two collimators, i.e., from 3 to 5 m of tungsten.

These considerations, based on qualitative arguments, are in agreement with the measured rates shown in Figs. 9(a) and 9(b).

Of course, the picture changes when crystals are used as primary collimation stage. A similar qualitative agreement is obtained when considering the different betatron phase advance between the various devices and collimator settings used with the crystal-collimation scheme, without forgetting the different coherent processes that are experienced in crystals.

IX. CONCLUSIONS

The operational use of crystal collimation in the LHC is achieved during a special high-β^* physics run, showing operational performance that represent a milestone for both accelerator and high-energy physics, which could pave the way for new synergies in the near future. The deployment of this scheme is steered and motivated by machine-simulation studies, which are then confirmed experimentally using data provided by the experiments thanks to a sensitivity not accessible with the instrumentation of the machine.

Crystals are aligned only during initial preparatory tests and automatically inserted in channeling orientation during the physics run. This proves the maturity reached by these powerful and innovative devices that can nowadays be used efficiently for beam manipulations in state-of-the-art machines, such as the LHC.

Data from the Roman pots show that the beam-related experimental background rate is significantly reduced at both experiments, leading also to an improved data quality with respect to what is obtained using amorphous collimators, in particular for TOTEM. Additional studies show that the distribution of beam-related background, which partially affected ALFA data quality, comes from a specific collimator—identified in simulations—and it is not intrinsically related to the use of bent crystals. Thus, operational settings can be further optimized in future runs based on crystal collimation.

The experimental observations of background rate stability, supported by simulation studies, indicates a faster halo removal with crystals with respect to amorphous collimators. Moreover, this background stability led to about 10% more collected luminosity per fill when using bent crystals, that represents an asset for this special runs to which only a few days of operations are dedicated.

A very good qualitative and quantitative agreement between predicted and measured background rate and distribution is obtained. This provides additional confidence in the accuracy of the available simulation tools, which can be reliably used to define operational scenarios for future applications of bent crystals at high-energy colliders that may be required by the high-energy physics community.

Low-intensity proton beams at injection energy are used in this special physics run. The main challenge presently left to make crystal collimation operational with high energy and intensity proton beams is the safe disposal of channeled halo particles in accident scenario. On the other hand, for the HL-LHC heavy-ion beams, this is not an issue as the total stored energy is of about 20 MJ. Crystal collimation for heavy-ion operation is therefore included in the HL-LHC baseline. Moreover, many other applications of this versatile technology are under study at CERN and in various laboratories, spanning over several applied physics domains.

APPENDIX A: ABBREVIATIONS

All abbreviations used throughout the paper are summarized below, in alphabetical order.

TABLE II. Operational settings of the LHC collimation system and Roman pots during the high-β^* physics run at 450 GeV in 2018. Nominal injection settings are reported, together with dedicated settings used during the data taking with the standard and crystal-collimation schemes. The crystal collimators are the devices TCPCV.A6[L/R]7.B[1/2]. Settings are expressed in units of RMS beam size (σ), assuming a Gaussian-beam distribution and normalized emittance $\varepsilon^* = 3.5$ μm.

Device	IR	Plane	Nominal injection (σ)	Standard collimation (σ)	Crystal collimation (σ)
TCL.4[R/L]1.B[1/2]	1	H	OUT	OUT	OUT
TCL.5[R/L]1.B[1/2]	1	H	OUT	OUT	OUT
TCL.6[R/L]1.B[1/2]	1	H	OUT	OUT	OUT
XRP.A7[R/L]1.B[1/2]	1	V	OUT	3.0	3.0
XRP.B7[R/L]1.B[1/2]	1	V	OUT	3.0	3.0
TCTPH.4[L/R]2.B[1/2]	2	H	13.0	13.0	13.0
TCTPV.4[L/R]2.B[1/2]	2	V	13.0	2.7	13.0
TDI.4[L/R][2/8].B[1/2]	2/8	V	6.8	OUT	OUT
TCLIA.4[L/R][2/8].B[1/2]	2/8	V	6.8	OUT	OUT
TCLIB.6[L/R][2/8].B[1/2]	2/8	V	6.8	OUT	OUT
TCP.6[L/R]3.B[1/2]	3	H	8.0	5.3	5.3
TCSG.5[L/R]3.B[1/2]	3	H	9.3	6.3	6.3
TCSG.4[R/L]3.B[1/2]	3	H	9.3	6.3	6.3
TCSG.A5[R/L]3.B[1/2]	3	S	9.3	6.3	6.3
TCSG.B5[R/L]3.B[1/2]	3	S	9.3	6.3	6.3
TCLA.A5[R/L]3.B[1/2]	3	V	12.0	2.7	2.7
TCLA.B5[R/L]3.B[1/2]	3	H	12.0	9.0	9.0
TCLA.6[R/L]3.B[1/2]	3	H	12.0	9.0	9.0
TCLA.7[R/L]3.B[1/2]	3	H	12.0	9.0	9.0
TCTPH.4[L/R]5.B[1/2]	5	H	13.0	13.0	13.0
TCTPV.4[L/R]5.B[1/2]	5	V	13.0	2.7	13.0/2.7
TCL.4[R/L]5.B[1/2]	5	H	OUT	OUT	OUT
TCL.5[R/L]5.B[1/2]	5	H	OUT	OUT	OUT
XRP.D6[R/L]5.B[1/2]	5	V	OUT	3.0	3.0
XRP.B6[R/L]5.B[1/2]	5	V	OUT	3.0	3.0
TCL.6[R/L]5.B[1/2]	5	H	OUT	OUT	OUT
TCDQ.4[R/L]6.B[1/2]	6	H	8.0	8.0	8.0
TCSP.A4[R/L]6.B[1/2]	6	H	7.5	7.5	7.5
TCP.D6[L/R]7.B[1/2]	7	V	5.7	3.2	3.2
TCP.C6[L/R]7.B[1/2]	7	H	5.7	4.0	4.0
TCP.B6[L/R]7.B[1/2]	7	S	5.7	5.7	5.7
TCSG.A6[L/R]7.B[1/2]	7	S	6.7	5.0	5.0
TCPCV.A6[L/R]7.B[1/2]	7	V	OUT	OUT	2.5
TCSG.B5[L/R]7.B[1/2]	7	S	6.7	5.0	5.0
TCSG.A5[L/R]7.B[1/2]	7	S	6.7	5.0	5.0
TCSG.D4[L/R]7.B[1/2]	7	V	6.7	5.0	5.0
TCSG.B4[L/R]7.B[1/2]	7	H	6.7	5.0	5.0
TCSG.A4[L/R]7.B[1/2]	7	S	6.7	5.0	5.0
TCSG.A4[R/L]7.B[1/2]	7	S	6.7	5.0	5.0
TCSG.B5[R/L]7.B[1/2]	7	S	6.7	5.0	5.0
TCSG.D5[R/L]7.B[1/2]	7	S	6.7	5.0	5.0
TCSG.E5[R/L]7.B[1/2]	7	S	6.7	5.0	5.0
TCSG.6[R/L]7.B[1/2]	7	H	6.7	5.0	5.0
TCLA.A6[R/L]7.B[1/2]	7	V	10.0	2.5	2.7
TCLA.B6[R/L]7.B[1/2]	7	H	10.0	8.0	8.0
TCLA.C6[R/L]7.B[1/2]	7	V	10.0	2.7	2.7
TCLA.D6[R/L]7.B[1/2]	7	H	10.0	10.0	10.0
TCLA.A7[R/L]7.B[1/2]	7	H	10.0	8.0	8.0
TCTPH.4[L/R]8.B[1/2]	8	H	13.0	13.0	13.0
TCTPV.4[L/R]8.B[1/2]	8	V	13.0	2.7	13.0
TCTPH.4[L/R]1.B[1/2]	1	H	13.0	13.0	13.0
TCTPV.4[L/R]1.B[1/2]	1	V	13.0	2.7	2.7/13.0

(a) ALFA: Absolute luminosity for ATLAS, forward physics detectors around ATLAS.

(b) ALICE: A large ion collider experiment, heavy-ion physics detector located at IP2.

(c) ATLAS: A toroidal LHC apparatus, multipurpose physics detector located at IP1.

(d) B1, B2: the two counterrotating beams in the LHC.

(e) BLM: Beam loss monitor.

(f) CMS: Compact muon solenoid, multipurpose physics detector located at IP5.

(g) HL-LHC: High-Luminosity Large Hadron Collider.

(h) IP: Interaction point.

(i) IR: Insertion region. The LHC has eight IRs. The experiments are located in IR1, IR2, IR5, and IR8. The main part of the collimation system is found in IR3 and IR7, the beam-extraction system is located in IR6, superconducting radio-frequency cavities are installed in IR4.

(j) LHC: Large Hadron Collider.

(k) LHCb: Large Hadron Collider beauty, flavor physics detector located at IP8.

(l) TCDQ: Target collimator dump quadrupole, single-sided mobile graphite diluter block used for beam dump protection in IR6 and made of 6.0-m-long jaw of graphite.

(m) TCL: Target collimator long, collimators used to absorb physics debris from the IP and made of 1-m-long jaws of tungsten.

(n) TCLA: Target collimator long absorber, collimators used to absorb hadronic showers developed in the first two collimation stages and made of 1-m-long jaws of tungsten. One of these collimators is used as the primary stage in the special high-β^* physics run presented in this Paper, when standard collimation is used.

(o) TCLIA and TCLIB: Target collimator long injection made of 1-m-long jaws of graphite, used to intercept out scattered particles from the TDI.

(p) TCP: Target collimator primary, collimators used as the primary stage during standard physics run and made of 60-cm-long jaws of carbon-fiber composite.

(q) TCPCV: Target collimator primary crystal vertical, bent crystals acting on the vertical plane and used as primary stage in the special high-β^* physics run presented in this Paper, made of 4-mm-long silicon crystal with 50 μrad bending.

(r) TCSG: Target collimator secondary, collimators used as the secondary stage during standard physics run and made of 1-m-long jaws of carbon-fiber composite.

(s) TCSP: Target collimator secondary equipped with beam-position monitor, secondary collimator used for beam dump protection in IR6 and made of 1-m-long jaws of carbon-fiber composite.

(t) TCTPH(V): Target collimator tertiary equipped with beam-position monitor acting on the horizontal (vertical) plane, collimator located in the experimental insertions as protection of sensitive equipment and made of 1-m-long jaws of tungsten.

(u) TDI: Target dump injection, absorber used for beam injection protection made of a composite jaw featuring 2.5-m graphite + 1-m aluminum + 0.7-m copper.

(v) TOTEM: Total cross section, elastic scattering and diffraction dissociation measurement; forward physics detectors around CMS.

(w) XRPV: Experimetal Roman pot acting on the vertical plane, used to house forward physics detectors around IP1 and IP5.

APPENDIX B: COLLIMATOR SETTINGS

The complete list of collimator settings used is reported in Table II.

[1] O. Brüning *et al.*, *LHC Design Report, Layout and Performance* (European Organization for Nuclear Research, Geneva, Switzerland, 2004).

[2] B. Salvachua *et al.*, in *LHC Beam Operations Workshop* (CERN, Evian, France, 2019).

[3] G. Antchev, P. Aspell, I. Atanassov, V. Avati, J. Baechler, C. B. Barrera, V. Berardi, M. Berretti, E. Bossini, U. Bottigli, *et al.*, First determination of the ρ parameter at $\sqrt{s} = 13$ TeV: Probing the existence of a colourless C-odd three-gluon compound state, Eur. Phys. J. C **79**, 785 (2019).

[4] H. Burkhardt, High-beta optics and running prospects, Instruments **3**, 22 (2019).

[5] H. Garcia Morales *et al.*, Tightest collimation system in the LHC (to be published).

[6] M. Gerard, T. Toshiki, and C. Swapan, in *Beam Acceleration in Crystals and Nanostructures-Proceedings of the Workshop* (World Scientific, 2020).

[7] V. Shiltsev, Experience with crystals at fermilab accelerators, Int. J. Mod. Phys. A **34**, 1943007 (2019).

[8] M. Oriunno, M. Deile, K. Eggert, J.-M. Lacroix, S. J. Mathot, E. P. Noschis, R. Perret, E. Radermacher, and G. Ruggiero, The roman pot for the LHC, Proc. EPAC **6**, 562 (2006).

[9] S. A. Khalek *et al.*, The ALFA roman pot detectors of ATLAS, J. Instrum. **11**, P11013 (2016).

[10] G. Anelli, G. Antchev, P. Aspell, V. Avati, M. Bagliesi, V. Berardi, M. Berretti, V. Boccone, U. Bottigli, M. Bozzo, *et al.*, The TOTEM experiment at the CERN large hadron collider, J. Instrum. **3**, S08007 (2008).

[11] W. Scandale and A. Taratin, Channeling and volume reflection of high-energy charged particles in short bent crystals. Crystal assisted collimation of the accelerator beam halo, Phys. Rep. **815**, 1 (2019).

[12] J. Jaeckel, M. Lamont, and C. Vallée, The quest for new physics with the physics beyond colliders programme, Nat. Phys. **16**, 393 (2020).

[13] C. Barschel, *Report from the LHC Fixed Target working group of the CERN Physics Beyond Colliders Forum*, Tech. Rep. CERN-PBC-REPORT-2019-001 (CERN, Geneva, 2019).

[14] D. Mirarchi, A. Fomin, S. Redaelli, and W. Scandale, Layouts for fixed-target experiments and dipole moment measurements of short-lived baryons using bent crystals at the LHC, Eur. Phys. J. C **80**, 1 (2020).

[15] N. Fuster Martinez, A. Abramov, G. Azzopardi, A. Gorzawski, E. Belli, C. Boscolo-Meneguolo, R. Bruce, M. D'Andrea, M. Di Castro, M. Fiascaris, *et al.*, in *LHC Beam Operations Workshop* (2019).

[16] R. Assmann, M. Magistris, O. Aberle, M. Mayer, F. Ruggiero, J. Jiménez, S. Calatroni, A. Ferrari, G. Bellodi, I. Kurochkin *et al.*, *The Final Collimation System for the LHC*, Tech. Rep. (2006).

[17] R. W. Assmann, in *Proceedings of the LHC Project Workshop − Chamonix XIV, Chamonix, France* 261 (CERN, Chamonix, France, 2005).

[18] R. Bruce, R. W. Assmann, V. Boccone, C. Bracco, M. Brugger, M. Cauchi, F. Cerutti, D. Deboy, A. Ferrari, L. Lari, *et al.*, Simulations and measurements of beam loss patterns at the CERN large hadron collider, Phys. Rev. Spec. Top.-Accelerators Beams **17**, 081004 (2014).

[19] G. Valentino, G. Baud, R. Bruce, M. Gasior, A. Mereghetti, D. Mirarchi, J. Olexa, S. Redaelli, S. Salvachua, A. Valloni, and J. Wenninger, Final implementation, commissioning, and performance of embedded collimator beam position monitors in the large hadron collider, Phys. Rev. Accelerators Beams **20**, 081002 (2017).

[20] D. Mirarchi, G. Hall, S. Redaelli, and W. Scandale, Design and implementation of a crystal collimation test stand at the large hadron collider, Eur. Phys. J. C **77**, 424 (2017).

[21] W. Scandale, G. Arduini, M. Butcher, F. Cerutti, M. Garattini, S. Gilardoni, A. Lechner, R. Losito, A. Masi, D. Mirarchi, *et al.*, Observation of channeling for 6500 GeV/c protons in the crystal assisted collimation setup for LHC, Phys. Lett. B **758**, 129 (2016).

[22] Y. M. Ivanov, A. Petrunin, and V. V. Skorobogatov, Observation of the elastic quasi-mosaicity effect in bent silicon single crystals, J. Exp. Theor. Phys. Lett. **81**, 99 (2005).

[23] HL-LHC Crystal Collimation Day, https://indico.cern.ch/event/752062/.

[24] A. Mazzolari, M. Romagnoni, E. Bagli, L. Bandiera, S. Baricordi, R. Camattari, D. Casotti, M. Tamisari, A. Sytov, V. Guidi, *et al.*, Silicon crystals for steering of high-intensity particle beams at ultra-high energy accelerators, arXiv:2006.15582 (2020).

[25] M. Garattini, Overview of crystal performance at SPS-H8, https://indico.cern.ch/event/752062/contributions/3114845/attachments/1737304/2810539/Garattini_CrystalSPS_H8.pdf (2018).

[26] M. D'Andrea, LHC operational experience with proton beams, https://indico.cern.ch/event/752062/contributions/3114848/attachments/1737254/2810510/MarcoDAndrea_CrystalCollimationDay2018_v5.pdf (2018).

[27] M. Butcher, A. Giustiniani, R. Losito, and A. Masi, in *Industrial Electronics Society, IECON 2015-41st Annual Conference of the IEEE* (IEEE, Yokohama, Japan, 2015), p. 003887.

[28] A. Masi, Goniometer and controls, https://indico.cern.ch/event/752062/contributions/3114861/attachments/1737557/2811350/CrystalCollimationDay19-10-2018HL-LHC_AM.pdf (2018).

[29] W. Scandale *et al.*, Channeling efficiency reduction in high dose neutron irradiated silicon crystals, The European Physical Journal C (Submitted, 2020).

[30] W. Scandale, M. Calviani, M. D'Andrea, L. Esposito, M. Garattini, S. Gilardoni, S. Montesano, A. Natochii, R. Rossi, G. Smirnov, *et al.*, Beam steering performance of bent silicon crystals irradiated with high-intensity and high-energy protons, Eur. Phys. J. C **79**, 1 (2019).

[31] C. Bahamonde, Crystal channeling of ions on different TCSG materials, https://indico.cern.ch/event/740297/contributions/3056136/attachments/1686653/2712474/ColUSM_106_-_Crystal_channeling_of_ions_on_different_TCSG_materials.pdf (2018).

[32] D. Quartullo, Updates on the longitudinal impedance of the LHC V2 goniometer, https://indico.cern.ch/event/921426/contributions/3871224/attachments/2047851/3431508/quartullo_2020_05_27_ColUSM.pdf (2020).

[33] M. D'Andrea, Preliminary results from crystal collimation studies in 2018, https://indico.cern.ch/event/804616/contributions/3347483/attachments/1812077/2959927/Crystals_TCC_MDAndrea_v2.pdf (2019).

[34] M. D'Andrea, Ph.D. thesis (to be published, 2020).

[35] O. Brüning, *High Luminosity LHC Technical Design Report*, Tech. Rep. (to be published, 2020).

[36] F. M. Velotti, L. S. Esposito, M. A. Fraser, V. Kain, S. Gilardoni, B. Goddard, M. Pari, J. Prieto, R. Rossi, W. Scandale, *et al.*, Septum shadowing by means of a bent crystal to reduce slow extraction beam loss, Phys. Rev. Accelerators Beams **22**, 093502 (2019).

[37] S. Redaelli, Experience with Multi-TeV Beam Channeling and Crystal Extraction at the LHC, https://indico.cern.ch/event/523655/contributions/2246436/attachments/1332375/2003150/SRedaelli_2016-09-06_print.pdf (2016).

[38] M. Tanabashi, K. Hagiwara, K. Hikasa, K. Nakamura, Y. Sumino, F. Takahashi, J. Tanaka, K. Agashe, G. Aielli, C. Amsler, *et al.*, Review of particle physics, Phys. Rev. D **98**, 030001 (2018).

[39] A. Denisov *et al.*, New measurements of the mass of the K-meson, JETP Lett. **54**, 558 (1991).

[40] M. Gurev *et al.*, First measurement of the X-ray emission of Sigma- atoms by means of a crystal diffraction spectrometer, JETP Lett. **57**, 400 (1993).

[41] W. Scandale, G. Arduini, M. Butcher, F. Cerutti, S. Gilardoni, A. Lechner, R. Losito, A. Masi, E. Metral, D. Mirarchi, *et al.*, Observation of focusing of 400 GeV/c proton beam with the help of bent crystals, Phys. Lett. B **733**, 366 (2014).

[42] W. Scandale, G. Arduini, F. Cerutti, M. Garattini, S. Gilardoni, A. Masi, D. Mirarchi, S. Montesano, S. Petrucci, S. Redaelli, *et al.*, Comprehensive study of beam focusing by crystal devices, Phys. Rev. Accelerators Beams **21**, 014702 (2018).

[43] W. Scandale, G. Arduini, F. Cerutti, M. Garattini, S. Gilardoni, A. Lechner, R. Losito, A. Masi, D. Mirarchi, S. Montesano, *et al.*, Focusing of 180 GeV/c pions from a point-like source into a parallel beam by a bent silicon crystal, Nucl. Instrum. Methods Phys. Res. Sect B **446**, 15 (2019).

[44] W. Scandale, G. Arduini, M. Butcher, F. Cerutti, S. Gilardoni, A. Lechner, R. Losito, A. Masi, E. Metral, D.

Mirarchi, *et al.*, Mirroring of 400 GeV/c protons by an ultra-thin straight crystal, Phys. Lett. B **734**, 1 (2014).

[45] Y. A. Chesnokov and V. Maisheev, Neutrino beams at ultra high energy proton colliders on the basis of focusing single crystals, Nucl. Phys. A **1003**, 122012 (2020).

[46] G. Britvich, A. Durum, M. Y. Kostin, V. Maisheev, Y. A. Chesnokov, and A. Yanovich, New method for the generation of secondary particle beams at accelerators, J. Exp. Theor. Phys. **129**, 229 (2019).

[47] N. Amapane, M. Antonelli, F. Anulli, G. Ballerini, L. Bandiera, N. Bartosik, M. Bauce, A. Bertolin, C. Biino, O. Blanco-Garcia, *et al.*, Study of muon pair production from positron annihilation at threshold energy, J. Instrum. **15**, P01036 (2020).

[48] Y. M. Shin, A. Green, A. Lumpkin, R. Thurman-Keup, V. Shiltsev, X. Zhang, D.-A. Farinella, P. Taborek, T. Tajima, J. Wheeler, *et al.*, in *AIP Conference Proceedings* Vol. 1812 (AIP Publishing LLC, National Harbor, Maryland, USA, 2017), p. 060009.

[49] U. Wienands, S. Gessner, M. Hogan, T. Markiewicz, T. Smith, J. Sheppard, U. Uggerhøj, J. Hansen, T. Wistisen, E. Bagli, *et al.*, Channeling and radiation experiments at SLAC, Nucl. Instrum. Methods Phys. Res. Sect B **402**, 11 (2017).

[50] L. Bandiera, E. Bagli, G. Germogli, V. Guidi, A. Mazzolari, H. Backe, W. Lauth, A. Berra, D. Lietti, M. Prest, *et al.*, Investigation of the Electromagnetic Radiation Emitted by sub-GeV Electrons in a Bent Crystal, Phys. Rev. Lett. **115**, 025504 (2015).

[51] A. V. Korol and A. V. Solov'Yov, Crystal-based intensive gamma-ray light sources, Eur. Phys. J. D **74**, 1 (2020).

[52] A. V. Pavlov, A. V. Korol, V. K. Ivanov, and A. V. Solov'Yov, Channeling of electrons and positrons in straight and periodically bent diamond (110) crystals, Eur. Phys. J. D **74**, 21 (2020).

[53] A. Mazzolari, E. Bagli, L. Bandiera, V. Guidi, H. Backe, W. Lauth, V. Tikhomirov, A. Berra, D. Lietti, M. Prest, *et al.*, Steering of a sub-GeV Electron Beam through Planar Channeling Enhanced by Rechanneling, Phys. Rev. Lett. **112**, 135503 (2014).

[54] M. Tabrizi, A. V. Korol, A. V. Solov'Yov, and W. Greiner, An electron-based crystalline undulator, J. Phys. G: Nucl. Part. Phys. **34**, 1581 (2007).

[55] A. Korol, A. Solov'Yov, and W. Greiner, Channeling of positrons through periodically bent crystals: On the feasibility of crystalline undulator and gamma-laser, Int. J. Mod. Phys. E **13**, 867 (2004).

[56] E. Virgilli, F. Frontera, P. Rosati, E. Caroli, N. Auricchio, and J. Stephen, in *The Fourteenth Marcel Grossmann Meeting* (World Scientific, Rome, Italy, 2018), p. 3289.

[57] E. Bagli, V. Guidi, and A. Howard, High-energy $e-/e+$ spectrometer via coherent interaction in a bent crystal, Astroparticle Phys. **97**, 27 (2018).

[58] E. Bagli and A. Howard, Towards a novel high energy $e-/e+$ charge spectrometer taking into account recent measurements of coherent interactions in a bent crystal, Nucl. Instrum. Methods Phys. Res. Sect A **936**, 216 (2019).

[59] W. Scandale, F. Cerutti, L. Esposito, M. Garattini, S. Gilardoni, A. Natochii, R. Rossi, G. Smirnov, V. Zhovkovska, F. Galluccio, *et al.*, Angular asymmetry of the nuclear

interaction probability of high energy particles in short bent crystals, Eur. Phys. J. C **80**, 1 (2020).

[60] E. Bagli, D. De Salvador, L. Bacci, F. Sgarbossa, L. Bandiera, R. Camattari, G. Germogli, A. Mazzolari, A. Sytov, and G. Guidi, Enhancement of the Inelastic Nuclear Interaction Rate in Crystals via Antichanneling, Phys. Rev. Lett. **123**, 044801 (2019).

[61] G. Germogli, D. D. Salvador, L. Bacci, E. Bagli, L. Bandiera, R. Camattari, S. M. Carturan, D. Casotti, F. Evangelisti, G. Guidi, *et al.*, Radioisotope production through accelerators in crystalline targets, Multidisciplinary Digital Publishing Inst. Proc. **26**, 51 (2019).

[62] C. Ray and D. Dauvergne, Proton and light ion deflection at medium energies with planar bent crystals, Nucl. Instrum. Methods Phys. Res. Sect B **402**, 313 (2017).

[63] B. S. Dziedzic and ATLAS Collaboration, *Measurement of beam background in special high-β^* LHC runs at $\sqrt(s) = 900 GeV$ using the ATLAS–ALFA detectors*, Tech. Rep. ATL-FWD-PUB-2020-001 (CERN, Geneva, 2020).

[64] J. Kašpar, Beam-background tests with TOTEM roman pot detectors at the LHC injection energy, Instruments **2**, 20 (2018).

[65] F. Schmidt, *SixTrack, User's Reference Manual*, Tech. Rep. (CERN SL/94-56 (AP), 1994).

[66] http://sixtrack.web.cern.ch/SixTrack/.

[67] G. Robert-Demolaize, R. Assmann, S. Redaelli, and F. Schmidt, in *Proceedings of the 2005 Particle Accelerator Conference* (IEEE, Knoxville, Tennessee, USA, 2005), p. 4084.

[68] http://lhc-collimation-project.web.cern.ch/lhc-collimation-project/code-tracking-2012.php.

[69] R. Bruce, C. Bracco, R. De Maria, M. Giovannozzi, A. Mereghetti, D. Mirarchi, S. Redaelli, E. Quaranta, and B. Salvachua, Reaching record-low β^* at the CERN large hadron collider using a novel scheme of collimator settings and optics, Nucl. Instrum. Methods Phys. Res. Sect A **848**, 19 (2017).

[70] R. Bruce, M. Huhtinen, A. Manousos, F. Cerutti, L. Esposito, R. Kwee-Hinzmann, A. Lechner, A. Mereghetti, D. Mirarchi, S. Redaelli, *et al.*, Collimation-induced experimental background studies at the CERN large hadron collider, Phys. Rev. Accelerators Beams **22**, 021004 (2019).

[71] V. Previtali, Ph.D. thesis, EPFL These N.4794, CERN-THESIS-2010-133 (2010).

[72] D. Mirarchi, Ph.D. thesis, Imperial College, London, CERN-THESIS-2015-099 (2015).

[73] D. Mirarchi, S. Redaelli, and W. Scandale, in *CERN Yellow Reports: Conference Proceedings* (CERN, 2018).

[74] D. Mirarchi, G. Hall, S. Redaelli, and W. Scandale, A crystal routine for collimation studies in circular proton accelerators, Nucl. Instrum. Methods Phys. Res. Sect B **355**, 378 (2015).

[75] W. Scandale, G. Arduini, M. Butcher, F. Cerutti, M. Garattini, S. Gilardoni, A. Lechner, R. Losito, A. Masi, A. Mereghetti, *et al.*, Observation of strong leakage reduction in crystal assisted collimation of the SPS beam, Phys. Lett. B **748**, 451 (2015).

[76] R. Rossi, Ph.D. thesis, CERN; INFN & University Roma I; CERN-THESIS-2017-424 (2017).

[77] W. Scandale, F. Andrisani, G. Arduini, F. Cerutti, M. Garattini, S. Gilardoni, A. Masi, D. Mirarchi, S. Montesano, S. Petrucci, *et al.*, Study of inelastic nuclear interactions of

400 GeV/c protons in bent silicon crystals for beam steering purposes, Eur. Phys. J. C **78**, 505 (2018).

[78] J. Kaspar, Observations in TOTEM, https://indico.cern.ch/event/775252/, mini-Workshop: Running LHC at injection energy.

[79] E. B. Holzer, B. Dehning, E. Effnger, J. Emery, V. Grishin, C. Hajdu, S. Jackson, C. Kurfuerst, A. Marsili, M. Misiowiec, *et al.*, Beam loss monitoring for LHC machine protection, Phys. Proc. **37**, 2055 (2012).

[80] M. Krupa and L. Soby, in *Proceedings of the 20th International Conference Mixed Design of Integrated Circuits and Systems-MIXDES 2013* (IEEE, Gdynia, Poland, 2013), p. 592.

[81] *TOTEM Upgrade Proposal*, Tech. Rep. CERN-LHCC-2013-009. LHCC-P-007 (CERN, Geneva, 2013).

[82] K. Osterberg, TOTEM Status Report, https://indico.cern.ch/event/771106/, 136th LHCC Meeting – OPEN Session.

[83] D. Mirarchi, Crystal collimation during high beta physics run, https://indico.cern.ch/event/770857/contributions/3202228/attachments/1751242/2838042/ColWG_cry_DM.pdf, LHC Collimation Working Group #235.